ELSEVIER

Journal of Molecular Catalysis A: Chemical 162 (2000) 83–95

JOURNAL OF MOLECULAR CATALYSIS A: CHEMICAL

www.elsevier.com/locate/molcata

# Chemical vapour deposition — a new approach to reactive surface defects of uniform geometry on high surface area magnesium oxide

E. Knözinger *, O. Diwald, M. Sterrer

*Institut für Physikalische und Theoretische Chemie, Technische Universität Wien, c/o Veterinärmedizinische Universität, Veterinärplatz 1/GA, A-1210, Wien, Austria*

**Abstract**

Chemical vapour deposition (CVD) is particularly well suited for the preparation of high surface area magnesium oxide which exhibits a considerably reduced surface heterogeneity. This is shown in the present study for three types of surface defects: low coordinated anions and cations as well as anion vacancies. For each of them, only two to three different species with discrete geometries are observed.

The characterization of these defects is based on specific EPR active molecular surface probes, namely, electron deficient oxygen anions $O^-$, superoxide anions $O_2^-$ and surface colour centres $F_S^+$, respectively. Some of the $O_2^-$ and $F_S^+$ centres exhibit a dipolar magnetic interaction with the proton of a closely spaced OH group. The electronic interaction is reflected by a change of the intramolecular force field of the respective OH group. Consequently, there is an IR spectroscopic access to the characterization of the defects in question. On the other hand, the surface $O^-$ species are absolutely insensitive to the hydroxylation state of the MgO surface. 

*Keywords:* Chemical vapour deposition; MgO; Surface defects; Surface reactivity; EPR; FTIR

## 1. Introduction

High surface area metal oxides, in general, exhibit an extremely irregular morphology. The microcrystals are terminated by several crystallographic planes which, thus, give rise to a considerable concentration of steps, kinks, edges and other defects, such as surface ion vacancies. All of them interrupt the bidimensional regularity, which can be attributed to the thermodynamically most favoured surface.

In the case of MgO, a highly ionic oxide with cubic structure, an enormous number of reports on vibrational [1–3] as well as EPR spectroscopic studies [4–7] have been published in the past. Hydrides and hydroxyl groups as surface probes originating from heterolytic splitting of $H_2$ on low-coordinated ion pairs were characterized by IR spectroscopy [8–10]. Surface hydroxyls play a most important role in catalysis as either acidic or basic sites [11]. The surface hydrides are not stable in the presence of $O_2$. This is due to an intermolecular electron transfer from the hydrides to $O_2$ molecules [12]. The resulting superoxide anion $O_2^-$ — if stable — is an efficient paramagnetic probe for the coordination state of surface cations [5,13,14]. The sites, where heterolytic $H_2$ splitting occurs, are also likely candidates as promotors for the heterolytic hydrogen ab-

* Corresponding author.
*E-mail address:* knoezinger@tuwien.ac.at (E. Knözinger).

1381-1169/00/$ - see front matter 
PII: S1381-1169(00)00323-X

straction from methane [15]. The resulting carbanions are susceptible to oxidation by $O_2$, and thus, are transformed into gaseous radical species, e.g. $CH_3^{\cdot}$, the educts of the coupling reaction [16].

Quite generally the generation of paramagnetic surface species is greatly facilitated by UV irradiation at $\lambda > 200$ nm. The respective quanta are energetic enough to transfer electrons and holes, but not ionic surface constituents. In pure MgO samples, the excitation process involves low coordinated surface anions ($O_{3C}^{2-}$ and $O_{4C}^{2-}$) [17] which undergo a charge transfer providing radical surface species:

$$O_{LC}^{2-} \xrightarrow{h\nu} O_{LC}^{-} + e^{-} \quad (1)$$

A reduction of the exciton excitation energy by decreasing the oxygen coordination has been corroborated by theoretical calculations [18]. $O_{LC}^{-}$ is responsible for homolytic $H_2$ splitting according to

$$O_{LC}^{-} + H_2 \rightarrow O_{LC}H^{-} + H^{\cdot} \quad (2)$$

UV light in the wavelength range 250–360 nm initiates photoadsorption of oxygen. Cation vacancies ($V_S^{2-}$) are likely surface sites on MgO where UV induced $O_3^-$ formation might occur [19].

Anion vacancies on magnesium oxide surfaces ($F_S^{2+}$) can be transformed into paramagnetic surface colour centres ($F_S^{+}$) via a UV induced electron transfer. Excellent candidates as electron donors are surface hydride groups [20,21]:

$$H^{-} + F_S^{2+} \xrightarrow{h\nu} H^{\cdot} + F_S^{+} \quad (3)$$

The same is true for neutral H atoms [22,23] which are produced according to Eq. (3) or by UV induced homolytic $H_2$ splitting (Eq. (2)):

$$H^{\cdot} + F_S^{2+} \xrightarrow{h\nu} H^{+} + F_S^{+} \quad (4)$$

There is an interesting interrelation between different classes of surface sites involved in the MgO surface reactions with $H_2$, $O_2$ and/or UV quanta. The low coordinated ions, which provide hydride groups and H atoms, are simple surface defects. The vacancies required for colour centre and ozonide production have then to be considered as composite defects incorporating several low coordinated ions.

A reliable spectroscopic characterization of all these defects on highly dispersed metal oxide surfaces necessarily implies a relevant abundance of the respective sites. Non-equilibrium techniques of metal oxide production such as precipitation from liquid solutions [24], thermal decomposition of hydroxide [25], and chemical vapour deposition (CVD) [26] have made specific surface areas of hundreds of $m^2/g$ available.

## 2. Experimental

All experiments were carried out with the same type of MgO obtained by chemical vapour deposition in a flow system [27]. High purity Mg pieces as educt were supplied by Johnson Matthey GmbH. The specific surface area of the resulting MgO material determined by BET ($LN_2$) measurements is around 400 $m^2/g$. In order to guarantee a totally dehydroxylated surface, the sample was gradually annealed at 1173 K under dynamic vacuum ($< 10^{-5}$ mbar) before each experiment. This leads to a reduction of the specific surface area to 320 $m^2/g$. The rate of temperature increase for the annealing steps was 10 K/min. All samples were treated at 870 K with oxygen in order to burn organic contaminants originating from the oil of the vacuum pumps used in the flow system. The gases $H_2$ (99.999%) and $^{16}O_2$ (99.998%) for adsorption studies were provided by Messer Griesheim. A 300 W Xe lamp (Oriel) was applied for UV irradiation. The light beam passes through a water filter in order to avoid sample heating by IR irradiation. All UV excitation experiments on MgO were carried out at room temperature. The exposure time amounted to 10 min in oxygen atmosphere and to 30 min in vacuo or in hydrogen (100 mbar, colour centre formation). Homolytic $H_2$ splitting on stable surface $O^-$ species was performed at 77 K and $H_2$ pressures below 0.5 mbar.

The IR and EPR sample cells are connected to an appropriate high vacuum pumping rack. It allows thermal activation of the sample at less than $10^{-5}$ mbar and adsorption/desorption experiments with diverse gases. For the IR experiments, small quantities of MgO powder (20–30 mg) were pressed into selfsupporting pellets. The pressure applied was less than 10 bar and did not initiate any change of the specific surface area. For the EPR experiments similar amounts of the MgO sample batch, also used for IR spectroscopy, was filled in EPR tubes.

The IR spectra were recorded using a Fourier-transform IR spectrometer model IFS 113v (Bruker Optik GmbH). The resolution was $3\,cm^{-1}$. Three hundred interferogram scans were averaged in order to guarantee a reasonable signal-to-noise ratio. The reference for the absorbance spectra is a MgO sample previously subjected to thermal activation and then cooled down to room temperature. The EPR spectra were recorded using a Bruker EMX 10/12 spectrometer system in the X-band. The colour centre signals were obtained at room temperature in one scan, whereas the spectra presenting paramagnetic oxygen species required a reduction of the temperature to 77 K, in order to avoid line broadening. In this case, 10 coadded spectra sufficed to obtain a satisfactory signal-to-noise ratio. The DPPH signal as well as the lines originating from traces of $Mn^{2+}$ in the sample were applied for g value calibration.

## 3. Specific surface properties of MgO nanoparticles emerging from chemical vapour deposition (CVD)

Different from thermal decomposition of the hydroxide which provides microcrystals with a platelike structure [28] CVD allows for the production of crystalline nanometer-sized MgO cubes. After thermal treatment at 900°C in vacuo they exhibit a surprisingly sharp size distribution (Fig. 1). The mean edge length of the cubes certainly depends on the CVD conditions applied. In Fig. 1, e.g. it amounts to 7 nm which corresponds to a specific surface area of around $300\,m^2/g$. Both morphology and surface structure of these MgO particles are retained on a time-scale of hours even at temperatures of 900°C (Fig. 2), whereas the isostructural CaO is strongly affected by sintering under the same conditions (Fig. 2). As predicted by theoretical calculations [29], MgO nanoparticles bearing a surface coverage of CaO exhibit an even higher thermal stability than the corresponding pure MgO sample (Fig. 2). The surface doped material is obtained by a thermally induced segregation process of a thermodynamically unstable MgO/CaO mixture originating from CVD [30]. This clearly shows the ample potential of CVD for further advancement in terms of the variation of metal oxide surface basicity.

The cubic shape of CVD MgO particles in the micrograph of Fig. 1 might suggest that the surface mainly comprises sites in flat (1 0 0) planes. This is certainly not true. On the contrary, the surface planes must host a considerable concentration of highly reactive defects. As an example in Fig. 3, the reactiv-

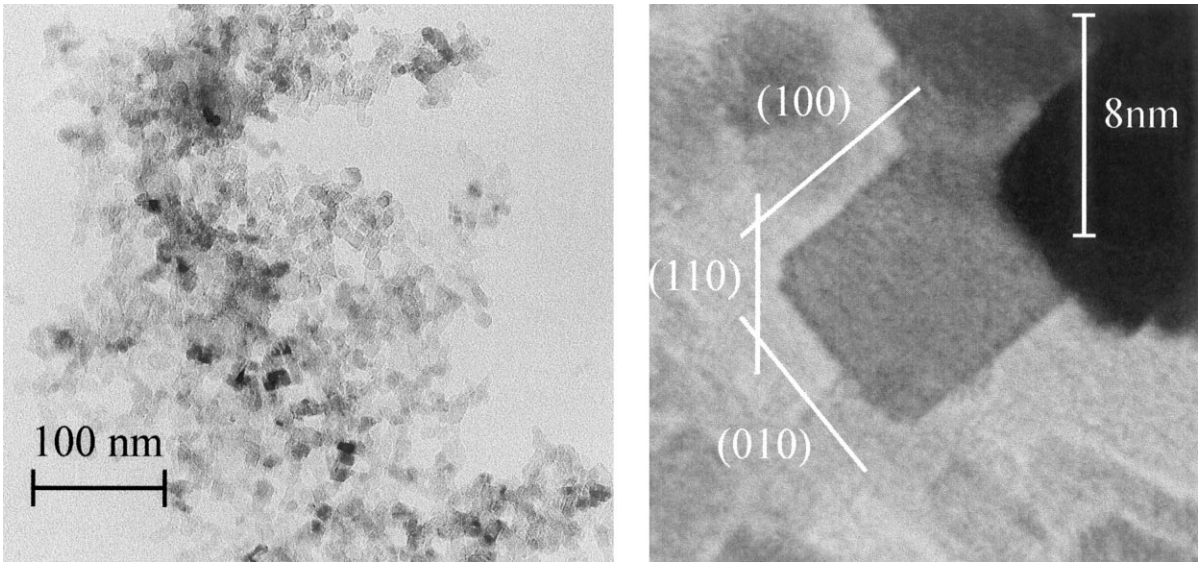


Fig. 1. Electron micrograph of CVD MgO after thermal pretreatment at 900°C in vacuo.

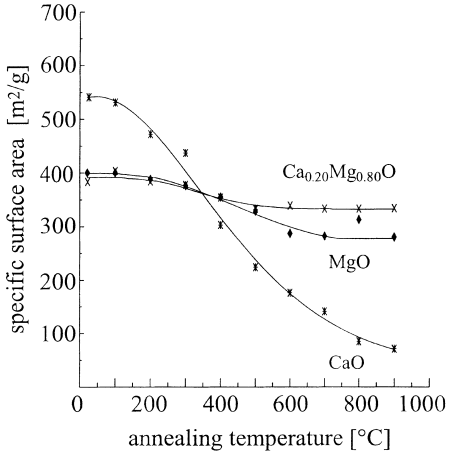


Fig. 2. Effect of thermal treatment in vacuo on the specific surface area (BET, $N_2$) of pure and surface doped alkaline earth oxides (used by permission [30]).

ities of isolated free surface OH groups on a CVD and on a commercial ex-hydroxide sample towards $D_2$ are compared [31]. The common pretreatment of both samples included a thermal activation at 900°C in vacuo, subsequent full hydroxylation at room temperature, and then, partial dehydroxylation at 600°C. The FTIR difference spectra clearly show the reactivity of the CVD sample (Fig. 3a) to be by at least two orders of magnitude higher than that of the ex-hydroxide sample (Fig. 3b), whereas the ratio of the respective surface areas amounts to only 5:1. This may be explained in terms of a CVD specific enrichment of low coordinated, and therefore, more reactive surface sites which tend to polarize the attached OH groups.

A realistic surface model of highly dispersed metal oxides may certainly not be based exclusively on a set of differently coordinated anions and cations. Single as well as multiple vacancies have to be adopted, too. There is conclusive experimental evidence that the non-equilibrium conditions of CVD also enrich the surface concentration of vacancies on the resulting MgO nanoparticles as compared to MgO originating from the other previously mentioned techniques [32].

In the course of our recent research activities, it turned out that certain surface states can be characterized by both EPR spectroscopy and — in an indirect way — by IR spectroscopy. Surface OH groups as IR active probes act as mediators between the sets of IR and EPR data. Their vibrational modes studied by FTIR react sensitively on physical and chemical particularities in their immediate environment, e.g. on the presence of more or less strong proton acceptors at a relevant distance [33]. On the other hand, the superhyperfine interaction between the nuclear spin of an OH proton and a closely spaced paramagnetic spin centre results in splitting effects of the respective EPR signals [34–36].

Such paramagnetic spin centres are surface colour centres $F_S^+$ and superoxide anions $O_2^-$ complexed by low coordinated surface cations. The $O_2^-$ species, themselves sensitively probe the coordination state of the complexing surface cation and reveal dramatic changes in the surface structure of CVD MgO during

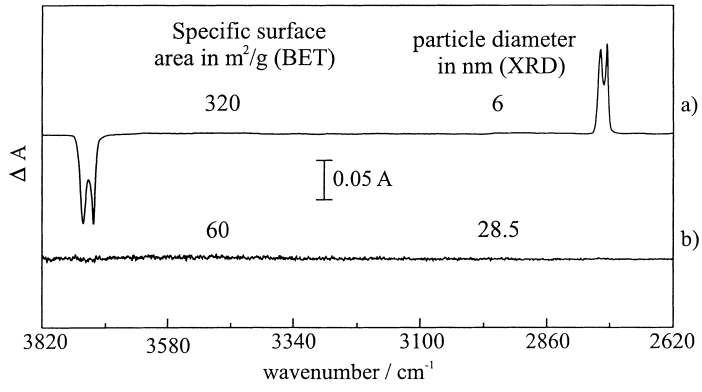


Fig. 3. IR difference spectra after reaction of free isolated surface hydroxyl groups with $D_2$ at room temperature (a) CVD sample (b) sample originating from calcination of $Mg(OH)_2$. Sample amount: 20 mg in either case; sample activation (see text).

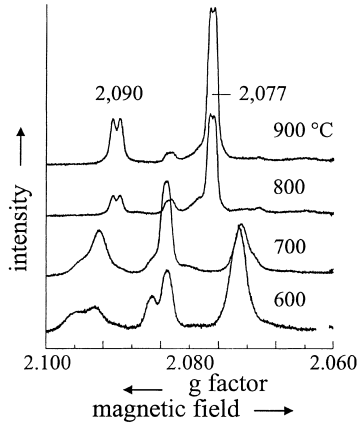


Fig. 4. Low field range ($g_{zz}$ components) of the EPR spectrum of $O_2^-$ species on CVD MgO after thermal activation at different temperatures.

the above mentioned thermal treatment. These changes are clearly reflected by the $g_{zz}$ components of the $O_2^-$ EPR signal (Fig. 4). Each peak corresponds to a characteristic surface cation coordination. Thus, the high complexity of the original unrelaxed surface fades away during thermal treatment at temperatures up to 800°C. On the other hand the remaining two cation sites still exhibit a considerable abundance and — in addition — thermal stability up to more than 900°C.

Obviously, the nanometer-sized MgO particles do not only exhibit essentially cubic shape, narrow size distribution and comparatively high surface defect concentration, but also a surprising degree of surface regularity: the fact that only two stable low-coordinated cation species survive the procedure of thermal treatment, provokes the assumption of a similar situation for the surface anions. Since the presence of surface vacancies necessarily implies the existence of low-coordinated surface ions as their constituents, the variety of different surface vacancies must also be very limited.

## 4. Chemistry and photochemistry on the surface of CVD MgO nanoparticles

Low coordinated surface ions are the sites from where the electron donors originate (Eqs. (3) and (4)), which are required for the formation of surface colour centres out of anion vacancies [20]. Efficient molecular probes for low coordinated surface ions are IR active OH (Table 1) and MgH groups. On the other hand, the EPR active paramagnetic colour centres are the unambiguous evidence for the presence of anion vacancies. Superoxide anions $O_2^-$ emerging during colour centre bleaching by $O_2$ are also EPR active and probe — once again — the coordination state of surface cations [5,13]. Another way of characterizing low-coordinated $O^{2-}$ anions is the charge transfer excitation to an $O^-$ radical which is EPR active and reacts with $H_2$ providing an IR active surface OH group [23]. Thus, the reactive interplay on the surface of CVD MgO gives rise to an interplay of two techniques of molecular spectroscopy, namely FTIR and EPR spectroscopy which — in a sense — appear to be complementary to each other. This complementarity as well as the regular surface structure and the high abundance of surface defects on CVD nanoparticles of MgO have provided the basis for a relevant advancement of chemistry and photochemistry on MgO surfaces. In the following the genesis and the properties of two MgO surface oxygen species which — most likely — play a prominent role in catalytic reactions such as oxidative coupling of methane (OCM) [16], will be reported: superoxide anions $O_2^-$ (Fig. 5, lower

Table 1
Vibrational frequencies of surface OH groups originating from diverse reactions on CVD MgO surfaces

| Band position ($cm^{-1}$) | Process | Type of OH group |
|---|---|---|
| 3712 | Heterolytic $H_2$ chemisorption | Free, isolated |
| 3698 | Homolytic $H_2$ chemisorption | Free, isolated |
| 3632/3602 | Colour centre formation | $OH\ldots F_S^+$ |
| 3528 | Colour centre formation | $OH\ldots F_S^+$ |
| 3692 | Colour centre bleaching | $OH\ldots O_2^-$ |
| 3702 | Colour centre bleaching | $OH\ldots O_2^-$ |

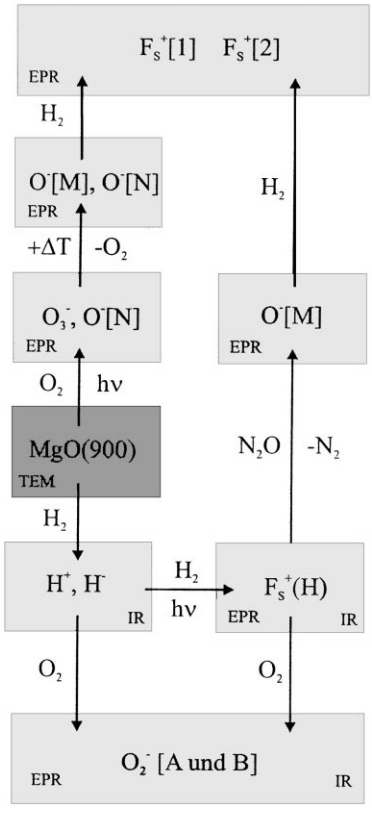


Fig. 5. Schematic representation of diverse elementary reaction steps on CVD MgO.

part) and electron deficient oxygen anions $O^-$ (Fig. 5, upper part).

### 4.1. Superoxide anions $O_2^-$

The starting point for the $O_2^-$ production is the fully dehydrated MgO exposed to molecular hydrogen ($H_2$) in the dark and at room temperature. It exhibits two types of chemisorption complexes (I and II) originating from heterolytic $H_2$ splitting on two different types of low-coordinated surface ion pairs which are thus transformed into an OH (Table 1) and a MgH group each [8–10]. The formation of complex II is an equilibrium process at room temperature whereas I is not. The abundance of surface sites related to II is — for an $H_2$ pressure $\geq$ 100 mbar — by at least an order of magnitude higher than that related to I. Both hydride species act as electron donors for the UV induced formation of surface colour centres $F_S^+$ out of anion vacancies according to Eq. (3) [20,21]. The presence of an OH group in the immediate environment is clearly evidenced by both EPR and IR spectroscopy. The superhyperfine splitting of the EPR signal [34,36] reflects the magnetic interaction between the OH proton and the unpaired colour centre electron. In order to recall the influence of the OH proton, this very classical surface colour centre was designated $F_S^+(H)$ [36]. IR bands at 3632, 3602 and 3528 $cm^{-1}$, i.e. in the range, where H bonded surface OH groups appear (Fig. 7a, left), indicate the electronic H-bond like interaction between a colour centre electron and a neighbouring surface OH group. Obviously, IR spectroscopy more sensitively responds to the interaction than cw EPR spectroscopy: there is only one type of superhyperfine splitting detected, whereas three well resolved IR bands are observed (Table 1). One of them (3528 $cm^{-1}$) exhibits a strong intensity increase on raising the $H_2$ pressure during colour centre formation. This increase correlates with the $H_2$ pressure dependence of the yield of the corresponding spin centre obtained by quantitative analysis of the EPR spectrum. We may, therefore, conclude, that there is one type of $F_S^+(H)$ centre of dominating surface concentration — namely $F_S^+(H)$ — and a less abundant second type which interacts with one out of two different OH groups.

The bleaching process of the $F_S^+(H)$ centres by $O_2$ addition occurs instantaneously: the magnesium oxide sample loses its blue colour and the $F_S^+(H)$ related signal in the EPR spectrum as well as the corresponding characteristic set of IR bands disappear [33]. Instead relevant new EPR and IR features are observed. A broad, moderately structured continous IR absorption in the spectral interval between 3650 and 3100 $cm^{-1}$ (Fig. 6a) points to the raised local surface concentration of OH groups which are incorporated in a complicated H bond network. It should be recalled here that heterolytic $H_2$ splitting (band at 3712 $cm^{-1}$, Fig. 6a and b, Table 1) as well as the UV induced processes of colour centre formation (bands at 3632/3602 and 3528 $cm^{-1}$, Fig. 7a, left) and of homolytic $H_2$ splitting (band at 3698 $cm^{-1}$, Fig. 6a) produce surface OH groups [23]. More specific spectral changes related to colour centre bleaching occur in the interval where essentially free isolated OH groups absorb (around

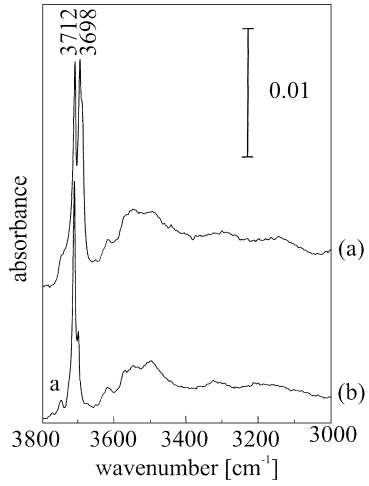


Fig. 6. IR spectrum (OH stretching region) of CVD MgO after surface reaction with $O_2$. MgO previously subjected to (a) UV induced surface colour centre formation; (b) $H_2$ splitting in the dark.

3700 $cm^{-1}$). Owing to considerable spectral congestion, it is extremely difficult to unravel this pattern as such. In the difference mode (Fig. 7a, left), where the original spectrum related to the state before the bleaching process is subtracted from that obtained thereafter, the evaluation is considerably less complicated: the negative bands related to the elimination of the colour centre influence on surface hydroxyl groups (3632, 3602 and 3528 $cm^{-1}$) are confronted with two relatively sharp, overlapping positive bands at 3702 and 3692 $cm^{-1}$ (Table 1). With respect to the isolated free OH group which absorbs at 3712 $cm^{-1}$, these bands are slightly shifted to smaller wave numbers, and thus, reflect an extremely weak interaction.

The character of the interaction partner of the OH groups is definitely revealed by EPR spectroscopy (Fig. 7a, right). During the bleaching process the $F_S^+(H)$ signal is replaced by a typical pattern related to the orthorhombic spin distribution of superoxide anion species. Obviously, the bleaching process may be described by an electron transfer from a colour centre $F_S^+(H)$ to an $O_2$ molecule giving rise to the formation of a superoxide anion $O_2^-$ (Eq. (5)).

$$F_S^+(H) + Mg^{2+} + O_2 \rightarrow F_S^{2+} + Mg^{2+} \cdots O_2^- \quad (5)$$

This paramagnetic species is complexed by a surface cation and exhibits a $g_{zz}$ component, the position of which sensitively depends on the coordination state of the complexing cation [5]. The EPR spectrum

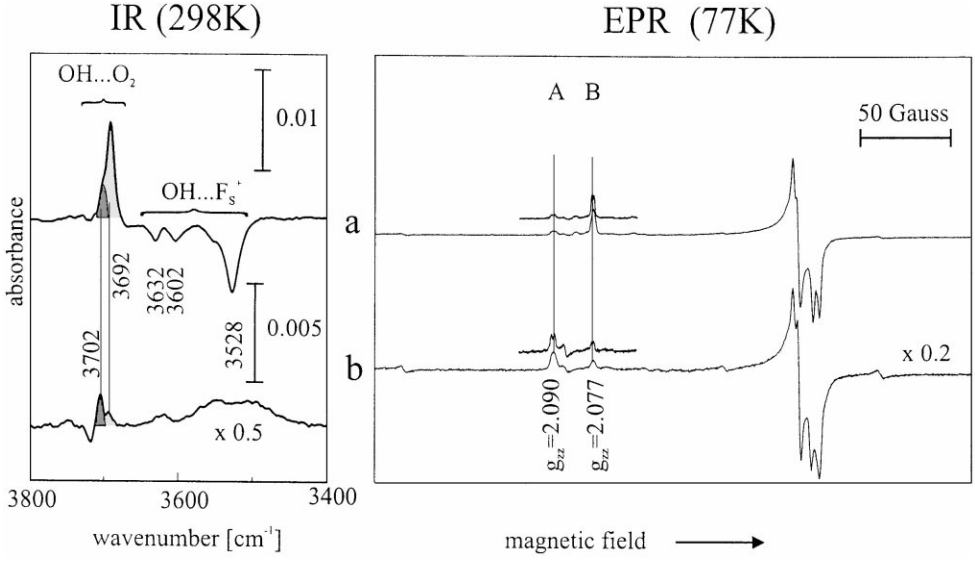


Fig. 7. (a) Surface colour centre bleaching by $O_2$ and (b) hydride induced $O_2$ chemisorption observed by IR difference spectroscopy (left) and by EPR spectroscopy (right). For quantitative comparison of ordinate values in a and b, the given factors have to be applied.

(Fig. 7a, right) clearly shows that there are at least two such surface complexes cation/$O_2^-$, called A and B. The relative abundance of A and B (obtained by spectral simulation of the low field region of the EPR spectrum) is in good agreement with the one of the two OH species absorbing at 3702 and 3692 $cm^{-1}$ (obtained by fitting and integration of the IR bands), respectively (Fig. 7a, left). This provides relevant clues as to the character of the interaction partner of the two OH groups in question: $O_2^-$ is an extremely weak proton acceptor, it is, however, the only one available after the elimination of the surface colour centre.

The dark reaction between $O_2$ and surface hydride groups provides two IR difference bands and two EPR $g_{zz}$ signal components (Fig. 7b) at precisely the same spectral positions as those observed in the colour centre bleaching experiment (Fig. 7a). Differences are observed for the relative abundance with the trends being the same for IR and EPR detection. In addition, the relative abundance of the underlying surface complexes also depends on the $H_2$ pressure during colour centre formation. Again the same trends are observed by EPR and IR spectroscopy [21].

Obviously, the same products — surface complexes OH... $O_2^-$[A] and OH... $O_2^-$[B] — are formed irrespective of the reaction path persued. This is even more surprising as UV quanta are involved in one of them only. A tentative explanation was based on the assumption that a relevant fraction of the surface centres responsible for heterolytic $H_2$ splitting and $O_2^-$ complexation are integral constituents or closely spaced neighbours of the anion vacancies which may be transformed into paramagnetic surface colour centres [20]. This is only true for the previously described $F_S^+$(H) centres of minor abundance (observed by IR spectroscopy). There is strong evidence that heterolytic $H_2$ splitting does not occur at the surface site attributed to the dominating type of $F_S^+$(H) centre [21] obtained according to Eq. (4) at high $H_2$ pressure and sufficiently long UV irradiation times.

One aspect in Fig. 7 has so far tacitly been neglected: the sample temperatures during the IR and EPR studies are different. The EPR spectra at 298 K exhibit a relatively unspecific structure owing to the mobility of the paramagnetic $O_2^-$ species which rotates or librates about axes perpendicular to its figure axis [37]. At 77 K all *g*-matrix components are sufficiently sharp to allow for a discrimination of the two $O_2^-$ species which are now rigidly embedded in well defined local surface elements. On the other hand, the IR detection of the $O_2^-$ species which is mainly based on Coulombic interaction between the unpaired $O_2^-$ electron and the proton of an OH group is essentially free from interference of $O_2^-$ mobility.

In both reaction paths — colour centre formation/colour centre bleaching by $O_2$ and dark reaction of $O_2$ with hydride — surface OH groups are produced by hydride oxidation, in addition to the OH groups originating from the initial heterolytic $H_2$ splitting. The local OH surface concentration is, therefore, considerably raised in the final state and a complicated H bond network between neighbouring OH groups appears to be likely. In fact, both reaction paths end up with moderately structured continuous IR absorptions in the spectral range where H bond affected OH groups show up (see above, Fig. 6a and b). The fascinating point is that the contours of these continuous features are very similar.[1] Obviously, the species which appear as end products on the surface much more depend on the intrinsic properties of the original virgin site than on the reaction path persued even though the respective energetics are dramatically different.

### *4.2. Electron deficient surface oxygen anions*

The prerequisite for the formation of $O^-$ species on the MgO nanoparticles is — as in the case of $O_2^-$ production (Section 4.1) — a fully dehydroxylated surface. From there two different reaction paths can be followed in order to create $O^-$ (Fig. 5). In the first one, the MgO sample is — as in Section 4.1 — simultaneously exposed to $H_2$ and UV light in order to create surface colour centres $F_S^+$(H) (Eq. (4)). Addition of $N_2O$ instead of $O_2$ bleaches the EPR signal of $F_S^+$(H) quantitatively and gives rise to a new EPR pattern (Fig. 8a) which is different from that obtained after $O_2$ bleaching (Fig. 7a, right). The

[1] Small but undisputable differences might be due to additional OH groups, which originate from the UV induced homolytic $H_2$ splitting accompanying colour centre formation.

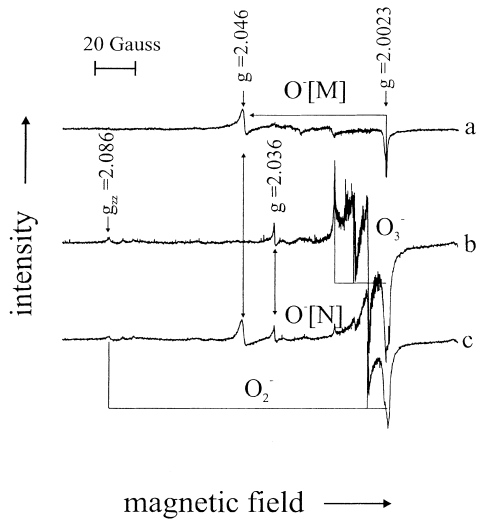


Fig. 8. EPR spectra of electron deficient surface anions produced by (a) colour centre bleaching via $N_2O$ addition; (b) UV induced $O_2$ chemisorption; (c) UV induced $O_2$ chemisorption and subsequent thermal treatment at 50°C.

components of the *g*-matrix have already been attributed previously to an electron deficient surface anion species $O^-$ in axial symmetry ($g_\perp = 2.046$, $g_\parallel = 2.002$, Table 2) [23]. As shown previously this $O^-$, which will be designated from now on $O^-[M]$, is not trapped or complexed by a single coordinatively unsaturated surface cation, but rather replaces the colour centre electron spin density in an anion vacancy [23] according to

$$F_S{}^+(H) + N_2O \rightarrow O^-[M] + N_2 \quad (6)$$

Different from the $F_S^+(H)$ centre which has disappeared, the EPR spectrum does not provide any clues as to a superhyperfine coupling with the proton of a closely spaced OH group (Fig. 8a).

$O_2$ does not react to any significant extent with the original fully dehydrated MgO surface — at least in the dark. Exposed to polychromatic UV light this material undergoes a photoinduced $O_2$ chemisorption which is evidenced without any doubt by EPR spectroscopy (Fig. 8b) and here we come across the second reaction path for the formation of $O^-$ (Fig. 5). A detailed analysis clearly evidenced the $g$ value components of both a surface ozonide species and of a second $O^-$ species with $g_\perp = 2.036$, $g_\parallel = 2.002$ [23] designated $O^-[N]$:

$$O_{LC}{}^{2-} + h\nu_{UV} + 2O_2 + Mg^{2+} \rightarrow O_3^- + Mg^{2+} \cdots O_2{}^- \quad (7)$$

$$O_{LC}{}^{2-} + h\nu_{UV} + O_2 + Mg^{2+} \rightarrow O^-[N] + Mg^{2+} \cdots O_2{}^- \quad (8)$$

By slightly heating the sample up to 323 K under dynamic vacuum, $O_3{}^-$ undergoes thermal decomposition into $O_2$ and $O^-[M]$ (Fig. 8c), the same $O^-[M]$ which was previously observed after colour centre

Table 2
*g*-Matrix components of paramagnetic species observed on CVD MgO surfaces

| Experimental | Predominant paramagnetic species | | *g*-matrix components | |
|---|---|---|---|---|
| $F_S{}^+ + UV, H_2$ | $F_S{}^+(H)$ | $g_\perp = 1.9997$ | $g_\parallel = 2.0013$ | |
| $F_S{}^+(H) + O_2$ | $O_2{}^-[A]$ | $g_{xx} = 2.0019$ | $g_{yy} = 2.0085$ | $g_{zz} = 2.090$ |
| | $O_2{}^-[B]$ | 2.0017 | 2.0086 | 2.077 |
| $F_S{}^+(H) + N_2O$ | $O^-[M]$ | $g_\perp = 2.046$ | $g_\parallel = 2.002$ | |
| $O_{LC}{}^{2-} + UV, O_2$ | $O^-[N]$ | 2.036 | 2.002 | |
| | $O_3{}^-$ | $g_{xx} = 2.0014$ | $g_{yy} = 2.018$ | $g_{zz} = 2.012$ |
| | $O_2{}^-$ | 2.0023 | 2.007 | $= 2.082/2.086$ |
| $O_3{}^- + \Delta T$ | $O^-[M]$ | $g_\perp = 2.046$ | $g_\parallel = 2.002$ | |
| $O^-[M] + H_2$ | $F_S{}^+[1]$ | 2.0004 | 2.0017 | |
| | $F_S{}^+[2]$ | 2.0007 | 2.0010 | |

bleaching with $N_2O$ (Fig. 8a). At the same time the EPR signal component $g_\perp = 2.036$ for $O^-[N]$ is essentially retained. This species is the result of a UV induced charge transfer on MgO surfaces ($\lambda > 200$ nm), which also occurs in high vacuum according to

$$O_{LC}{}^{2-} + h\nu_{UV} \rightarrow O_{LC}{}^{-} + e^- \quad (8a)$$

Under high vacuum the short-lived charge transfer complex consists of the localized hole $O^-[N]$ and a delocalized electron [38]. According to previous studies [23,39], $O^-[N]$ is attributed to a 3- or 4-coordinated oxygen ion. In the presence of $O_2$ gas, $O^-[N]$ is stabilized by trapping the electron of Eq. (8a) according to Eq. (8b):

$$Mg_{LC}{}^{2+} + e^- + O_2 \rightarrow Mg_{LC}{}^{2+} \cdots O_2^- \quad (8b)$$

The superoxide anions are complexed by low coordinated cations. The EPR spectrum of these $O_2{}^-$ species, in particular the $g_{zz}$ components, are clearly seen in Fig. 8b and c.

The comparison of the respective *g*-matrix components with those obtained in the course of the electron transfer processes presented in Section 4.1 (Fig. 7a and b, right; Table 2), indicates relevant differences. They must closely relate to the presence of hydroxyl groups on surfaces where $O_2$ has reacted with colour centres or hydride groups (Fig. 7, right), whereas OH groups do not participate at all in the process of the $O^-$ production via UV induced $O_2$ chemisorption (Fig. 8b and c). This assumption has been corroborated by a theoretical study demonstrating that $O_2{}^-$/cation complexes are significantly stabilized by neighbouring OH groups [40]. This could also explain the more specific $g_{zz}$ pattern in the case of the hydroxylated surface (Fig. 7a, right).

As described above, $O^-[M]$ may be created on MgO surfaces in the course of two fundamentally different reaction paths starting from fully dehydrated MgO nanoparticles: one of them is absolutely free from molecular hydrogen as reactant, the other one involves $H_2$ which is then — in several reaction steps — oxidized to surface OH groups. As the contours of the two $O^-[M]$ signals (Fig. 8a and c) do not exhibit any differences (compare the $g_\perp$ components at $g = 2.046$) we have to conclude, that the electron spin density is not affected by the presence of any type of neighbouring OH group. The other interesting point is that $O^-[M]$ either originates from the insertion of the $N_2O$ oxygen atom into a surface colour centre $F_S{}^+(H)$ or from thermal decomposition of surface ozonide which is preferentially formed at cation vacancies $V_S{}^{2-}$ [19] — provided the UV quanta and the $O_2$ molecules have simultaneous access to these sites. If the colour centre in question had emerged from a single anion vacancy on an edge or a corner the resulting $O^-$ species would be identical with $O^-[N]$. Recalling the fact, that surface ozonide production necessarily implies the presence of $V_S{}^{2-}$ centres, double vacancies appear to be likely candidates for the sites where $O^-[M]$ emerges after the reaction of $N_2O$ with a surface colour centre $F_S{}^+(H)$ (Fig. 10): the resulting $O^-[M]$ is constituent of a single cation vacancy $V_S{}^{2-}$ which is — see above — the prerequisite for UV induced formation of ozonide and — later on — of $O^-[M]$ [23].

According to Eq. (4) hydrogen in atomic form should react even in the dark with anion vacancies of sufficiently high electron affinity [41]. The $O^-$ species obtained in either of the two reaction paths discussed above are capable of homolytic $H_2$ splitting (Eq. (2)) even at 77 K [23]: the EPR spectrum after the reaction of $H_2$ with the $N_2O$ bleached surface shows a complex pattern (Fig. 9a, black curve). Quite obviously, more than one species resonate in this small range of magnetic field close to the free spin value. At first sight, only one attributable feature is recognized: the superhyperfine splitting of the $g_\perp$ component of the $F_S{}^+(H)$ centre (see Fig. 9a, arrows). In order to disentangle the composite signal, the microwave power was reduced from 100 to 10 μW (Fig. 9b) with the expectation that the most abundant species should gain relative intensity. In fact, the signal contour is only slightly changed: one single negative peak is significantly reinforced (see arrow, in Fig. 9b). We shall come back to it in the next paragraph.

The reaction of $H_2$ with the $O^-$ species prepared on the ozonide route (Fig. 8c) also provides a complex signal (Fig. 9a, grey curve) similar to the one described above (Fig. 9a, black curve). The $F_S{}^+(H)$ centre is not observed at all (arrows in Fig. 9a). At reduced MW power (10 μW compared to 100 μW) only one paramagnetic centre remains (Fig. 9b, grey curve). It exhibits axial symmetry. Computer simula-

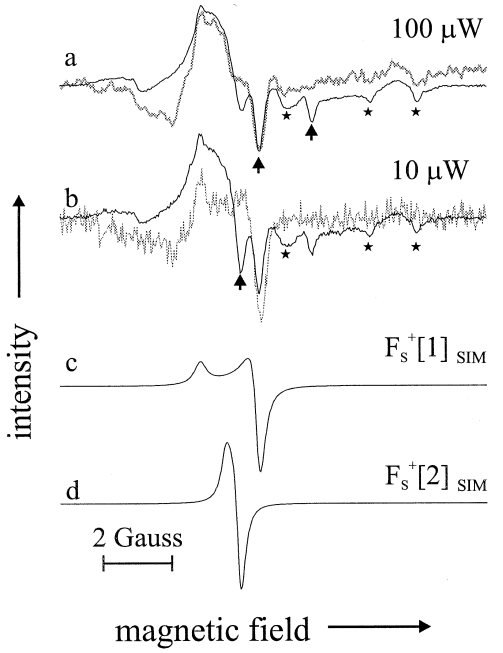


Fig. 9. EPR spectra of surface colour centres obtained by the reaction of $H_2$ with $O^-$ species (a and b). The $O^-$ species were previously produced by two different processes. Black curve: colour centre bleaching by $N_2O$. Grey curve: UV induced chemisorption of $O_2$ and subsequent heating at 50°C (grey curves are ordinate expanded by a factor of 30 as compared to black curves). (c) and (d) simulation carried out on the basis of the signal in (b). (The asterisks indicate the presence of unidentified paramagnetic species of minor abundance)

tion (Fig. 9c) provides the parameters of the *g*-matrix ($g_\perp = 2.004$, $g_{||} = 2.0017$) which are identical to those of a surface colour centre which does not allow for superhyperfine coupling with the proton of a closely spaced OH group [23]. It is designated here $F_S^+[1]$. The comparison of Fig. 9c with the black curve of Fig. 9a indicates without any doubt the presence of $F_S^+[1]$ also after the reaction of $H_2$ with $N_2O$ bleached surfaces. The comparison of the black curves in Fig. 9a and b then clearly evidences a third contribution to the composite pattern. Computer simulation provides the nearly symmetric signal presented in Fig. 9d. It exhibits the *g*-matrix values $g_\perp = 2.0007$ and $g_{||} = 2.0010$ and is designated $F_S^+[2]$ (Table 2).

Both, $F_S^+[1]$ and $F_S^+[2]$ are not subject to any superhyperfine coupling effects, and thus, indicate the absence of a distinct interaction with a nearby hydroxyl group. The uncharged, and therefore, surface mobile H atom of Eq. (2) is finally trapped as electron donor for anion vacancies:

$$F_S^{2+} + O^{2-} + H^\cdot \rightarrow F_S^+ + OH^- \quad (9)$$

The local ionic constituents of the resulting colour centres do obviously not comprise an appropriate low coordinated $O^{2-}$ for the formation of an OH group suitable for superhyperfine coupling (Fig. 10). $F_S^+[1]$ and $F_S^+[2]$ appear to be the predominant types of colour centres which originate in the dark out of the reaction between an H atom and an anion vacancy of comparatively high electron affinity: the H atom is ionized. Most interestingly, the electron affinity of the anion vacancy which leads to the $F_S^+(H)$ centre, does not suffice to ionize an H atom. The assistance of UV quanta is needed in order to promote this ionization process to the extent generally observed [20,21,34]. An alternative explanation for the absence of $F_S^+(H)$ centres after the reaction of $H_2$ with $O^-$ species obtained on the ozonide route is based on the blockade of anion vacancies by

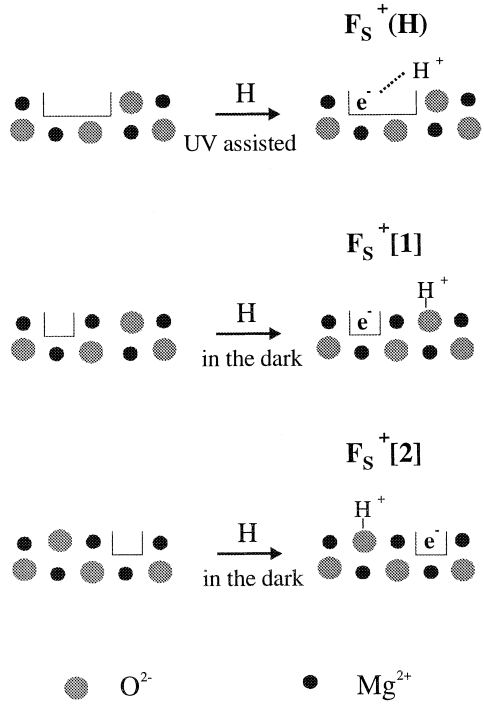


Fig. 10. Schematic representation of the diverse types of surface anion vacancies on CVD MgO which may be transformed into surface colour centres.

complexation of the respective cation constituents with $O_2^-$ species.

## 5. Conclusion

It has to be emphasized that CVD MgO greatly facilitates the spectroscopic characterization of surface defects and their derivatives. $H_2$ chemisorption — in the dark as well as under UV irradiation — creates well defined reduced surface sites which then react with $O_2$. Both the reduction as well as the subsequent oxidation step can be controlled by FTIR and EPR spectroscopy.

In preliminary studies, we have shown that single reactive surface sites may selectively be activated by properly tuned monochromatic light [39]. This enables the role of specific reaction steps to be reliably controlled. In addition, only recently experimental evidence was obtained in our laboratory which indicates that the reactive surface centres involved in $H_2$ splitting are the same as those initiating hydrogen abstraction from methane [39]. In all probability, a subsequent oxidation step by $O_2$ should then occur in agreement with that observed after $H_2$ splitting. Thus, the access of EPR and FTIR spectroscopy to all of the participants in the diverse parallel and subsequent reaction steps opens up new horizons for relevant mechanistic studies of such interesting reactions as oxidative coupling of methane [16].

## Acknowledgements

The authors are indebted to Dr. Michael Giersig (HMI, Berlin) for providing the transmission electron micrograph presented in Fig. 1. Considerable financial support from the Fonds zur Förderung der wissenschaftlichen Forschung (Contract No. P 11542-CHE) and the Max-Buchner-Stiftung (Contract No. H-00027/95) is gratefully acknowledged.

## References

[1] H.-P. Boehm, H. Knözinger, Catal. Sci. Technol. 4 (1983) 39.
[2] S. Lavagnino, S. Coluccia, L. Marchese, Mater. Chem. Phys. 174 (1988) 342.
[3] A. Zecchina, D. Scarano, S. Bordiga, in: G. Ertl, H. Knözinger, J. Weitkampp, V.C.H. Weinheim (Eds.), Handbook of Heterogenous Catalysis, Vol. 2, 1997, 838 pp.
[4] M. Che, A.J. Tench, Adv. Catal. 31 (1982) 77.
[5] M. Che, A.J. Tench, Adv. Catal. 32 (1983) 1.
[6] D. Murphy, E. Giamello, Mol. Eng. 4 (1994) 147.
[7] M. Che, E. Giamello, Stud. Surf. Sci. Catal. 57B (1990) 265.
[8] S. Coluccia, F. Boccuzzi, G. Ghiotti, C. Mirra, Zeitschrift für Physikalische Chemie Neue Folge 121 (1980) 141.
[9] S. Coluccia, F. Boccuzzi, G. Ghiotti, C. Morterra, J. Chem. Soc., Faraday Trans. I 78 (1982) 2111.
[10] E. Knözinger, K.H. Jacob, P. Hofmann, J. Chem. Soc. Faraday Trans. I 89 (1993) 1101.
[11] H. Knözinger, in: G. Ertl, H. Knözinger, J. Weitkampp, V.C.H. Weinheim (Eds.), Handbook of Heterogenous Catalysis, Vol. 2, 1997, 707 pp.
[12] E. Garrone, E. Giamello, M. Ferraris, G. Spoto, J. Chem. Soc., Faraday Trans. 88 (1992) 333.
[13] M. Anpo, M. Che, B. Fubini, E. Farrone, E. Giamello, M.C. Paganini, Topics Catal. 8 (1999) 189.
[14] E. Giamello, P. Ugliengo, E. Garrone, J. Chem. Soc., Faraday Trans. I 85 (1989) 1373.
[15] T. Ito, T. Watanabe, T. Tashiro, K. Toi, J. Chem. Soc., Faraday Trans. I 85 (1989) 2381.
[16] J.H. Lunsford, in: G. Ertl, H. Knözinger, J. Weitkampp, V.C.H. Weinheim (Eds.), Handbook of Heterogenous Catalysis, Vol. 4, 1997, 1843 pp.
[17] E. Garrone, A. Zechina, F.S. Stone, Phil. Mag. B 42 (1980) 683.
[18] A.L. Shluger, Phys. Rev. B 59 (1999) 2417.
[19] A.J. Tench, N. Kaufherr, Proceedings of the 6th International Congress on Catalysts, 1976, Vol. 1, 1977, 182 pp.
[20] E. Giamello, M.C. Paganini, M. Chiesa, S. Coluccia, G. Martra, D. Murphy, G. Pacchioni, Surf. Sci. 421 (1999) 246.
[21] O. Diwald, P. Hofmann, E. Knözinger, Phys. Chem. Chem. Phys. 1 (1999) 713.
[22] T. Ito, M. Kato, K. Toi, T. Shirakawa, I. Ikemoto, T. Tokuda, J. Chem. Soc., Faraday Trans. I 81 (1985) 2835.
[23] M. Sterrer, O. Diwald, E. Knözinger, J. Phys. Chem. B 104 (2000) 3601.
[24] K.J. Klabunde, J. Stark, O. Koper, C. Mohs, D.G. Park, S. Decker, Y. Jiang, I. Lagadic, D. Zhang, J. Phys. Chem. 100 (1996) 12142.
[25] S. Coluccia, M. Baricco, L. Marchese, G. Martra, A. Zecchina, Spectrochim. Acta 49A (1993) 1289.
[26] A. Becker, S. Benfer, P. Hofmann, K.-H. Jacob, E. Knözinger, Ber. Bunsenges. Phys. Chem. 99 (1995) 1328.
[27] E. Knözinger, K.-H. Jacob, S. Singh, P. Hofmann, Surf. Sci. 290 (1993) 388.
[28] S. Coluccia, M. Baricco, L. Marchese, G. Martra, A. Zecchina, Spectrochim. Acta 49A (1993) 1289.
[29] P.W. Tasker, E.A. Colbourn, W.C. Mackrodt, J. Am. Ceram. Soc. 68 (1985) 74.
[30] P. Hofmann, E. Knözinger, O. Diwald, A. Mustafa: Ber. Bunsenges. Phys. Chem. 101 (1997) 1722.
[31] S. Benfer, P. Hofmann, E. Knözinger, J. Mol. Struct. 115 (1997) 410.

[32] O. Diwald, E. Knözinger, unpublished results.
[33] O. Diwald, E. Knözinger, G. Martra, J. Chem. Phys. 111 (1999) 6668.
[34] E. Giamello, M.C. Paganini, D.M. Murphy, A.M. Ferrari, G. Pacchioni, J. Phys. Chem. B 101 (1997) 971.
[35] E. Giamello, P. Ugliengo, E. Garrone, J. Chem. Soc., Faraday Trans. I 85 (1989) 1373.
[36] D. Murphy, R.D. Farley, I.J. Purnell, C.C. Rowlands, A.R. Yacob, M.C. Paganini, E. Giamello, J. Phys. Chem. B 103 (1999) 1944.
[37] K. Dyrek, A. Adamski, Z. Sojka, Spectrochim. Acta A 54 (1998) 2337.
[38] P.V. Sushko, A.L. Shluger, C.R.A. Catlow, Surf. Sci. 450 (2000) 153.
[39] O. Diwald, M. Sterrer, E. Knözinger, in preparation.
[40] N.U. Zhanpeisov, G.M. Zhidomirov, Mendeleev Commun. 2/00992 (1992) 111.
[41] D.R. Smith, A.J. Tench, Chem. Com. 1113 (1968).